PERGAMON

International Journal of Solids and Structures 39 (2002) 1463–1486

INTERNATIONAL JOURNAL OF SOLIDS and STRUCTURES

www.elsevier.com/locate/ijsolstr

A two-dimensional closed-form solution for the free-vibrations analysis of piezoelectric sandwich plates

Ayech Benjeddou *, Jean-François Deü

Structural Mechanics and Coupled Systems Laboratory, Conservatoire National des Arts et Métiers, Chaire de Mécanique, 2 rue Conté, 75003 Paris, France

Received 23 April 2001; received in revised form 17 October 2001

Abstract

This work presents a two-dimensional (2D) closed-form solution for the free-vibrations analysis of simply-supported piezoelectric sandwich plates. It has the originality to consider all components of the electric field and displacement, thus satisfying exactly the electric equilibrium equation. Besides, the formulation considers full layerwise first-order shear deformation theory and through-thickness quadratic electric potential. Its independent mechanical and electric variables are decomposed using Fourier series expansions, then substituted in the derived mechanical and electric 2D equations of motion. The resulting eigenvalue system is then condensed so that only nine mechanical unknowns are retained. After its validation on single- and three-layer piezoelectric, and hybrid sandwich plates, the present approach was then used to analyze thickness modes of a square sandwich plate with piezoceramic faces and elastic cross-ply composite core. It was found that only the first three thickness modes are global, thus can be modeled by the mixed equivalent single-layer/layerwise approach, often retained in the literature; the remaining higher thickness modes being characteristic of sandwich behavior; i.e., dominated by the deformations of either the core or the faces. These results, together with presented through-thickness variations of the mechanical and electric variables clearly recommend full layerwise modeling. Several numerical results are provided for future reference for validation of 2D approximate analytical or numerical approaches; in particular, of 2D piezoelectric adaptive finite elements.

Keywords: Analytical solutions; Vibration; Piezoelectric; Adaptive structures; Simply-supported; Plate; Sandwich theory; Quadratic electric potential

1. Introduction

Several three-dimensional (3D) analytical solutions have been proposed in the literature for the free-vibrations analysis of simply-supported piezoelectric laminated plates (Saravanos and Heyliger, 1999). Hence, the well known Srinivas et al. (1970) exact solution for elastic laminates has been extended to piezoelectric ones (Heyliger and Saravanos, 1995). Therefore, an eighth-order frequency equation has been

* Corresponding author. Fax: +33-1-4027-2716.
E-mail address: benjedou@cnam.fr (A. Benjeddou).

0020-7683/02/$ - see front matter
PII: S0020-7683(01)00287-6

obtained, but its explicit exact solution was very lengthy and complicated. Moreover, due to the ill-conditioned resulting non-linear eigenvalue problem, the zero-determinant requirement was recognized to be very difficult to satisfy numerically. Later, the previous procedure, based on exponential expansions of the transverse dependence of all variables, has been simplified by assuming through-thickness linear electric potential in each lamina (Batra and Liang, 1997). Thus, a sixth-order frequency equation has been obtained. The piezoelectric layers were supposed so thin that they have been considered as membranes. However, both solutions (Heyliger and Saravanos, 1995; Batra and Liang, 1997) have the advantage to present explicit representations of their fundamental variables transverse variations.

In contrary to above approaches, only implicit representation of the independent variables transverse dependence can be obtained using the state space approach (Xu et al., 1997). Here, also the electric potential was assumed linear. It is then worthy to notice that the latter two solutions (Batra and Liang, 1997; Xu et al., 1997) did not satisfy exactly the electric charge equation. Moreover, the electromechanical coupling was represented only implicitly since there was no electric fundamental variable in their respective formulations. A new state space formulation had then been proposed recently (Ding et al., 2000). It retains the electric potential and transverse displacement as state variables, and has the advantage to lead to lower order than previous conventional eighth-order state equations.

Analytical two-dimensional (2D) solutions for the free-vibration analysis of simply-supported piezoelectric laminated plates have been presented in the literature only as application examples of other theoretical (Mitchell and Reddy, 1995; Shen and Kuang, 1999; Krommer and Irschik, 2000) or numerical (Correia et al., 2000) analyses. These consider only through-thickness components of the electric field and/or displacement. Moreover, all of them were based on mixed equivalent single layer (ESL) theory and layerwise modeling of the mechanical and electric behaviors, respectively. Hence, the third-order shear deformation theory was retained by Mitchell and Reddy (1995), Shen and Kuang (1999) and Correia et al. (2000) together with a layerwise linear or quadratic (Mitchell and Reddy, 1995), linear (Shen and Kuang, 1999) and uniform or linear (Correia et al., 2000) electric potential for the piezoelectric layers of the laminated plate. However, Krommer and Irschik (2000) have combined the Reissner–Mindlin plate theory with a layerwise quadratic electric potential to study the direct piezoelectric and pyroelectric effects.

As shown in the previous literature analysis, full 2D electromechanical layerwise modeling, retaining all components of the electric field and displacement, has not yet been considered for the free-vibration analysis of simply-supported piezoelectric laminated plates. Therefore, it is the aim of the present work to propose a 2D closed-form solution for the free-vibrations analysis of simply-supported piezoelectric sandwich plates. These are of practical use in vibration control of plates with either surface-mounted or embedded piezoelectric actuators and/or sensors. The theoretical formulation is based on Mindlin theory and through-thickness quadratic electric potential for each layer. Besides, all components of the electric field and displacement are retained. Thanks to the displacement interface continuities, the fundamental variables are reduced to in-plane face displacements and rotations, plate transverse deflection, and electric potential constants of each piezoelectric layer. Hence, an explicit representation of the piezoelectric effect is achieved and the full electromechanical coupling is maintained. Each of the previous fundamental variables is next decomposed using Fourier series expansions, then substituted in the 2D electromechanical equations of motion, derived from the extended principle of virtual works (Benjeddou, 2000a) using stress and electric displacement resultants. The resulting eigenvalue problem is then condensed so that it is reduced to a standard one in terms of only nine unknown mechanical constants.

In the following, the electromechanical basic equations and corresponding variational formulation are first presented. Then, the closed-form solution associated to the simply-supported piezoelectric sandwich plate formulation is derived. This includes the equations of motion and the derivation of the eigenvalue problem equation. The proposed approach is first verified through vibration analyses of single- and three-layer piezoelectric, and hybrid sandwich plates. Then, thickness modes of a square sandwich plate with piezoceramic faces and elastic cross-ply composite core are presented and analyzed.

2. Piezoelectric sandwich plate formulation

Consider the three-layer sandwich plate represented on Fig. 1. All layers are assumed piezoelectric, through-thickness polarized and can have different thickness and material properties. They are supposed to respect Mindlin plate theory assumptions. The electric potential is considered quadratic in each layer. The whole plate is supposed simply supported so that transverse and tangential displacements vanish at the boundaries. Its vertical edges are supposed potential- and stress-free. For the vibration problem in hand, the upper and lower surfaces are considered stress- and electric potential- or charge-free.

2.1. Basic equations

Following above assumptions, a linear displacement field is retained for the kth layer,

$$\begin{aligned} u_x^k(x,y,z,t) &= u^k(x,y,t) + (z-\overline{z}_k)\beta_x^k(x,y,t) \\ u_y^k(x,y,z,t) &= v^k(x,y,t) + (z-\overline{z}_k)\beta_y^k(x,y,t) \\ u_z^k(x,y,z,t) &= w(x,y,t) \end{aligned} \tag{1}$$

where $z \in [z_k, z_{k+1}]$, $\overline{z}_k = (z_k + z_{k+1})/2$ and $k = 1, 2, 3$. u^k, v^k, w, β_x^k, β_y^k are the kth layer mid-surface displacements along x, y, z and rotations in x–z and y–z planes, respectively.

In each layer, the linear strains are derived from above equation using the usual strain–displacement relations. Nevertheless, the transverse normal strains are deduced from the zero-normal stress assumption of the first-order shear deformation theory (FSDT) so that only five strain components are retained,

$$\begin{aligned} &\varepsilon_{xx}^k = e_{xx}^k + (z-\overline{z}_k)\chi_{xx}^k, \quad \varepsilon_{yy}^k = e_{yy}^k + (z-\overline{z}_k)\chi_{yy}^k, \quad \gamma_{xy}^k = e_{xy}^k + (z-\overline{z}_k)\chi_{xy}^k \\ &\gamma_{yz}^k = w_{,y} + \beta_y^k, \quad \gamma_{xz}^k = w_{,x} + \beta_x^k \end{aligned} \tag{2}$$

with

$$\begin{aligned} &e_{xx}^k = u_{,x}^k, \quad e_{yy}^k = v_{,y}^k, \quad e_{xy}^k = u_{,y}^k + v_{,x}^k; \\ &\chi_{xx}^k = \beta_{x,x}^k, \quad \chi_{yy}^k = \beta_{y,y}^k, \quad \chi_{xy}^k = \beta_{x,y}^k + \beta_{y,x}^k \end{aligned}$$

where "$,\alpha$" denoting the space partial differentiation with respect to $\alpha = x, y$.

The electric potential is assumed through-thickness quadratic in each layer so that,

$$\phi^k(x,y,z,t) = \phi_0^k(x,y,t) + (z-\overline{z}_k)\phi_1^k(x,y,t) + (z-\overline{z}_k)^2\phi_2^k(x,y,t) \tag{3}$$

Substituting this equation in the usual electric field–potential relation, the electric field in the kth layer can be written as,

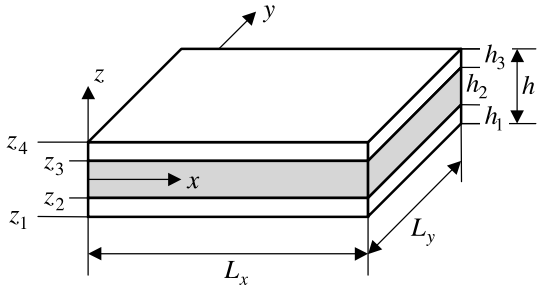

Fig. 1. The piezoelectric sandwich plate: geometry and notations.

$$E_x^k = E_{0x}^k + (z-\overline{z}_k)E_{1x}^k + (z-\overline{z}_k)^2 E_{2x}^k; \quad E_y^k = E_{0y}^k + (z-\overline{z}_k)E_{1y}^k + (z-\overline{z}_k)^2 E_{2y}^k$$
$$E_z^k = E_{0z}^k + (z-\overline{z}_k)E_{1z}^k \tag{4}$$

with

$$E_{0x}^k = -\phi_{0,x}^k,\ E_{1x}^k = -\phi_{1,x}^k,\ E_{2x}^k = -\phi_{2,x}^k; \quad E_{0y}^k = -\phi_{0,y}^k,\ E_{1y}^k = -\phi_{1,y}^k,\ E_{2y}^k = -\phi_{2,y}^k;$$
$$E_{0z}^k = -\phi_1^k,\ E_{1z}^k = -2\phi_2^k$$

Mechanical strain and electric field components are coupled through linear converse and direct piezoelectric constitutive equations given by,

$$\sigma_{ij}^k = C_{ijmn}^k \varepsilon_{mn}^k - e_{lij}^k E_l^k$$
$$D_i^k = e_{imn}^k \varepsilon_{mn}^k + \epsilon_{il}^k E_l^k \tag{5}$$

where C_{ijmn}^k, e_{imn}^k, ϵ_{il}^k $(i,j,l,m,n = x,y,z)$ are the elastic, piezoelectric and dielectric constants. σ_{ij}^k, D_i^k are the stress and electric displacement components. They satisfy the following mechanical and electric equations of harmonic motions,

$$\sigma_{ij,j}^k = -\rho^k \omega^2 u_i^k$$
$$D_{i,i}^k = 0 \tag{6}$$

where ω is the circular frequency (rad/s).

The plate is considered simply supported so that its transverse and tangential displacements vanish at its vertical edges,

$$u_y^k = u_z^k = 0 \quad \text{at } x = 0, L_x$$
$$u_x^k = u_z^k = 0 \quad \text{at } y = 0, L_y \tag{7}$$

The lower, upper and lateral surfaces of the sandwich plate are supposed stress free so that,

$$\sigma_{iz}^1 = 0 \quad \text{at } z = -\frac{h}{2}; \quad \sigma_{iz}^3 = 0 \quad \text{at } z = +\frac{h}{2}$$
$$\sigma_{xx}^k = 0 \quad \text{at } x = 0, L_x; \quad \sigma_{yy}^k = 0 \quad \text{at } y = 0, L_y \tag{8}$$

Electrically, the plate is either short- or open- (charge-free) circuited at its upper/lower surfaces, and short-circuited (potential-free) at its vertical edges,

$$\phi^{1,3} = 0 \quad \text{or} \quad D_z^{1,3} = 0 \quad \text{at } z = \pm\frac{h}{2} \tag{9a}$$

$$\phi^k = 0 \quad \text{at } x = 0, L_x \quad \text{and} \quad y = 0, L_y \tag{9b}$$

The displacements should be made continuous at the sandwich interfaces, in order to observe perfect bonding between the layers. That is,

$$u_i^1 = u_i^2 \quad \text{at } z = z_2$$
$$u_i^3 = u_i^2 \quad \text{at } z = z_3 \tag{10}$$

Fundamentally, the transverse stresses should be also made continuous at the sandwich plate interfaces so that,

$$\begin{aligned} \sigma_{iz}^1 &= \sigma_{iz}^2 \quad \text{at } z = z_2 \\ \sigma_{iz}^3 &= \sigma_{iz}^2 \quad \text{at } z = z_3 \end{aligned} \tag{11}$$

However, due to FSDT assumptions (layerwise constant shear and zero-normal stresses), previous equations could be satisfied only a posteriori, using the 3D electromechanical equilibrium equations.

Electrically, all layers are assumed conductive and not electroded on their inner faces. Hence, the electric potentials should be made continuous at the sandwich plate interfaces,

$$\begin{aligned} \phi^1 &= \phi^2 \quad \text{at } z = z_2 \\ \phi^3 &= \phi^2 \quad \text{at } z = z_3 \end{aligned} \tag{12}$$

To respect perfect electric bonding (no interface electrodes), the electric displacements have also to satisfy the following electric continuity conditions,

$$\begin{aligned} D_z^1 &= D_z^2 \quad \text{at } z = z_2 \\ D_z^3 &= D_z^2 \quad \text{at } z = z_3 \end{aligned} \tag{13}$$

As for the transverse stress continuity conditions, Eq. (11), the previous electric displacement ones could be enforced only a posteriori. This is again due to the electromechanical coupling and the FSDT assumptions regarding the normal and transverse shear stresses.

The local electromechanical vibration problem in hand consists of finding the harmonic displacements and electric potentials satisfying all previous equations, except Eqs. (11) and (13).

2.2. Variational formulation

The variational formulation of the vibration problem in hand is based on the virtual work principle, extended to piezoelectric media (Tiersten, 1969; Benjeddou, 2000a). For admissible virtual displacements and electric potentials, this can be written for the piezoelectric sandwich plate as,

$$\sum_{k=1}^{3} \left[\int_{\Omega^k} (\delta\varepsilon_{ij}^k \sigma_{ij}^k - \delta E_i^k D_i^k)\, \mathrm{d}\Omega^k - \omega^2 \int_{\Omega^k} \delta u_i^k \rho^k u_i^k\, \mathrm{d}\Omega^k \right] = 0 \tag{14}$$

with σ_{ij}^k, D_i^k satisfying Eq. (5). $\delta\varepsilon_{ij}^k$, δE_i^k follow Eqs. (2) and (4), respectively. The displacement and electric potential solutions are constrained to verify boundary, Eqs. (7) and (9a, first term), and continuity, Eqs. (10) and (12), conditions; whereas, the stress and electric displacement solutions have to satisfy boundary conditions, Eqs. (8) and (9b, second term), only.

To reduce the previous variational equation to a 2D one, the following stress resultants and moments are introduced for the kth layer,

$$N_{\alpha\beta}^k = \int_{z_k}^{z_{k+1}} \sigma_{\alpha\beta}^k\, \mathrm{d}z, \quad Q_{\alpha z}^k = \int_{z_k}^{z_{k+1}} \sigma_{\alpha z}^k\, \mathrm{d}z, \quad M_{\alpha\beta}^k = \int_{z_k}^{z_{k+1}} (z - \overline{z}_k)\sigma_{\alpha\beta}^k\, \mathrm{d}z \tag{15}$$

The zero, first and second order inertia moments are classically defined as,

$$(I_0^k, I_1^k, I_2^k) = \int_{z_k}^{z_{k+1}} [1, (z - \overline{z}_k), (z - \overline{z}_k)^2] \rho^k\, \mathrm{d}z \tag{16}$$

Zero, first and second order electric displacement resultants are similarly introduced,

$$(\overline{D}_{0i}^k, \overline{D}_{1i}^k) = \int_{z_k}^{z_{k+1}} [1, (z - \overline{z}_k)] D_i^k\, \mathrm{d}z, \quad \overline{D}_{2\alpha}^k = \int_{z_k}^{z_{k+1}} (z - \overline{z}_k)^2 D_\alpha^k\, \mathrm{d}z \tag{17}$$

The 2D variational equation of the vibration problem in hand results from the combined use of Eqs. (15)–(17) and the through-thickness explicit integration of Eq. (14),

$$\sum_{k=1}^{3}\left[\int_A(\delta e^k_{\alpha\beta}N^k_{\alpha\beta}+\delta\chi^k_{\alpha\beta}M^k_{\alpha\beta}+\delta\gamma^k_{\alpha z}Q^k_{\alpha z})\,\mathrm{d}A-\int_A(\delta E^k_{0z}\overline{D}^k_{0z}+\delta E^k_{1z}\overline{D}^k_{1z}+\delta E^k_{j\alpha}\overline{D}^k_{j\alpha})\,\mathrm{d}A\right.$$
$$\left.-\omega^2\int_A[(\delta u^k_{0\alpha}I^k_0u^k_{0\alpha}+\delta wI^k_0w)+(\delta u^k_{0\alpha}I^k_1\beta^k_\alpha+\delta\beta^k_\alpha I^k_1u^k_{0\alpha})+\delta\beta^k_\alpha I^k_2\beta^k_\alpha]\,\mathrm{d}A\right]=0 \tag{18}$$

where u_{0x}, u_{0y} state for u, v, respectively, and A is the plate middle surface area. Notice that the inertia virtual work (second line of Eq. (18)) contains all translation, rotary and their coupling inertia contributions. It is worthy to recall that the electromechanical coupling is present in the previous variational equation through the stress and electric displacement resultants. These include in fact both mechanical and electric contributions. Hence, from the zero-normal stress reduced piezoelectric constitutive equations (cf. Appendix A) and the stress resultants, the following generalized membrane-bending and transverse shear converse piezoelectric constitutive equations can be written,

$$\begin{Bmatrix}\mathbf{N}\\ \mathbf{M}\end{Bmatrix}^{(k)}=\begin{bmatrix}\mathbf{A}&\mathbf{B}\\ \mathbf{B}&\mathbf{D}\end{bmatrix}^{(k)}\begin{Bmatrix}\mathbf{e}\\ \boldsymbol{\chi}\end{Bmatrix}^{(k)}-\begin{bmatrix}\mathbf{F}&\mathbf{G}\\ \mathbf{G}&\mathbf{H}\end{bmatrix}^{(k)}\begin{Bmatrix}E_{0z}\\ E_{1z}\end{Bmatrix}^{(k)} \tag{19a}$$

$$\begin{Bmatrix}Q_{xz}\\ Q_{yz}\end{Bmatrix}^{(k)}=h_k\begin{bmatrix}C_{55}&0\\ 0&C_{44}\end{bmatrix}^{(k)}\begin{Bmatrix}\gamma_{xz}\\ \gamma_{xz}\end{Bmatrix}^{(k)}-\begin{bmatrix}\mathbf{P}_x&\mathbf{0}\\ \mathbf{0}&\mathbf{P}_y\end{bmatrix}^{(k)}\begin{Bmatrix}\mathbf{E}_x\\ \mathbf{E}_y\end{Bmatrix}^{(k)} \tag{19b}$$

with

$$\langle\mathbf{N}\rangle^{(k)}=\langle N_{xx}\ N_{yy}\ N_{xy}\rangle^{(k)},\quad \langle\mathbf{M}\rangle^{(k)}=\langle M_{xx}\ M_{yy}\ M_{xy}\rangle^{(k)}$$
$$\langle\mathbf{e}\rangle^{(k)}=\langle e_{xx}\ e_{yy}\ e_{xy}\rangle^{(k)},\quad \langle\boldsymbol{\chi}\rangle^{(k)}=\langle\chi_{xx}\ \chi_{yy}\ \chi_{xy}\rangle^{(k)}$$
$$\langle\mathbf{E}_\alpha\rangle^{(k)}=\langle E_{0\alpha}\ E_{1\alpha}\ E_{2\alpha}\rangle^{(k)}$$

and

$$[\mathbf{A}]^{(k)}=h_k[\mathbf{C}^*]^{(k)},\quad [\mathbf{B}]^{(k)}=\frac{(h_k)^2}{2}[\mathbf{C}^*]^{(k)},\quad [\mathbf{D}]^{(k)}=\frac{(h_k)^3}{12}[\mathbf{C}^*]^{(k)}$$

$$\{\mathbf{F}\}^{(k)}=h_k\{\mathbf{e}^*_t\}^{(k)},\quad \{\mathbf{G}\}^{(k)}=\frac{(h_k)^2}{2}\{\mathbf{e}^*_t\}^{(k)},\quad \{\mathbf{H}\}^{(k)}=\frac{(h_k)^3}{12}\{\mathbf{e}^*_t\}^{(k)}$$

$$\langle\mathbf{P}_x\rangle^{(k)}=\left\langle h_k\frac{(h_k)^2}{2}\frac{(h_k)^3}{12}\right\rangle C^k_{55},\quad \langle\mathbf{P}_y\rangle^{(k)}=\left\langle h_k\frac{(h_k)^2}{2}\frac{(h_k)^3}{12}\right\rangle C^k_{44}$$

Similarly, from the zero-normal stress reduced piezoelectric constitutive equations (cf. Appendix A) and the electric displacement resultants, the following generalized transverse and in-plane direct piezoelectric constitutive equations are obtained,

$$\begin{Bmatrix}\overline{D}_{0z}\\ \overline{D}_{1z}\end{Bmatrix}^{(k)}=\begin{bmatrix}\mathbf{F}^T&\mathbf{G}^T\\ \mathbf{G}^T&\mathbf{H}^T\end{bmatrix}^{(k)}\begin{Bmatrix}\mathbf{e}\\ \boldsymbol{\chi}\end{Bmatrix}^{(k)}+\begin{bmatrix}R_{00}&R_{01}\\ R_{01}&R_{11}\end{bmatrix}^{(k)}\begin{Bmatrix}E_{0z}\\ E_{1z}\end{Bmatrix}^{(k)} \tag{20a}$$

$$\begin{Bmatrix}\overline{D}_{jx}\\ \overline{D}_{jy}\end{Bmatrix}^{(k)}=\frac{(h_k)^{j+1}}{j+1}\begin{bmatrix}e_{15}&0\\ 0&e_{24}\end{bmatrix}^{(k)}\begin{Bmatrix}\gamma_{xz}\\ \gamma_{yz}\end{Bmatrix}^{(k)}-\begin{bmatrix}\mathbf{R}_x&0\\ 0&\mathbf{R}_y\end{bmatrix}^{(k)}\begin{Bmatrix}\mathbf{E}_x\\ \mathbf{E}_y\end{Bmatrix}^{(k)} \tag{20b}$$

with

$$R^k_{00} = h_k \epsilon^{*k}_{33}, \quad R^k_{01} = \frac{(h_k)^2}{2}\epsilon^{*k}_{33}, \quad R^k_{11} = \frac{(h_k)^3}{12}\epsilon^{*k}_{33}$$

$$\langle \mathbf{R}_\alpha \rangle^{(k)} = \left\langle \frac{(h_k)^{j+1}}{j+1} \frac{(h_k)^{j+2}}{j+2} \frac{(h_k)^{j+3}}{j+3} \right\rangle \epsilon^k_{\alpha\alpha}$$

The modified elastic matrix $[\mathbf{C}^*]$, piezoelectric coupling vector $\{\mathbf{e}^*_t\}$ and modified dielectric constant ϵ^*_{33} are given in Appendix A.

3. Closed-form solution

A displacement harmonic solution, respecting boundary conditions (7) and (8, second part) is,

$$\begin{aligned} u^k(x,y,t) &= U^k \cos px \sin qy \exp(\mathrm{i}\omega t); \quad \beta^k_x(x,y,t) = B^k_x \cos px \sin qy \exp(\mathrm{i}\omega t) \\ v^k(x,y,t) &= V^k \sin px \cos qy \exp(\mathrm{i}\omega t); \quad \beta^k_y(x,y,t) = B^k_y \sin px \cos qy \exp(\mathrm{i}\omega t) \\ w(x,y,t) &= W \sin px \sin qy \exp(\mathrm{i}\omega t) \end{aligned} \tag{21}$$

where, $p = m_x\pi/L_x$, $q = m_y\pi/L_y$, $\mathrm{i}^2 = -1$. m_x, m_y are non-negative integer mode numbers. This solution should also respect the continuity conditions of Eq. (10). Therefore, the core displacement and rotation constants can be expressed in terms of those of the faces,

$$\begin{aligned} U^2 &= \frac{1}{2}(U^3 + U^1) + \frac{1}{4}(h_1 B^1_x - h_3 B^3_x); \quad B^2_x = \frac{U^3 - U^1}{h_2} - \frac{1}{2}\left(\frac{h_1}{h_2}B^1_x + \frac{h_3}{h_2}B^3_x\right) \\ V^2 &= \frac{1}{2}(V^3 + V^1) + \frac{1}{4}(h_1 B^1_y - h_3 B^3_y); \quad B^2_y = \frac{V^3 - V^1}{h_2} - \frac{1}{2}\left(\frac{h_1}{h_2}B^1_y + \frac{h_3}{h_2}B^3_y\right) \end{aligned} \tag{22}$$

so that the unknown mechanical variables of the vibration problem in hand reduce to,

$$U^1, V^1, \mathrm{B}^1_x, \mathrm{B}^1_y, W, U^3, V^3, \mathrm{B}^3_x, \mathrm{B}^3_y \tag{23}$$

An electric potential harmonic solution that satisfies the boundary condition (9b) can be obtained by choosing its jth ($j = 0, 1, 2$) in-plane function in the form,

$$\phi^k_j(x,y,t) = \Phi^k_j \sin px \sin qy \exp(\mathrm{i}\omega t) \tag{24}$$

As for the mechanical constants, the electric ones could be reduced thanks to the electric potential boundary, Eq. (9a, first term), and continuity, Eq. (12), conditions. Hence, for short-circuited upper and lower plate electrodes, the following relations hold,

$$\begin{aligned} \Phi^1_0 &= \frac{h_1}{2}\Phi^1_1 - \left(\frac{h_1}{2}\right)^2 \Phi^1_2, \quad \Phi^2_0 = \frac{h_1}{2}\Phi^1_1 - \frac{h_3}{2}\Phi^3_1 - \left(\frac{h_2}{2}\right)^2 \Phi^2_2 \\ \Phi^3_0 &= -\frac{h_3}{2}\Phi^3_1 - \left(\frac{h_3}{2}\right)^2 \Phi^3_2, \quad \Phi^2_1 = -\frac{h_1}{h_2}\Phi^1_1 - \frac{h_3}{h_2}\Phi^3_1 \end{aligned} \tag{25}$$

This reduces the unknown electric variables of the electromechanical vibration problem to,

$$\Phi^1_1, \Phi^1_2, \Phi^2_2, \Phi^3_1, \Phi^3_2 \tag{26}$$

For open-circuited upper and lower plate electrodes, Eq. (9a, second term), only continuity conditions, Eq. (12), hold, leading to the following relations,

$$\begin{aligned}\Phi_0^1 &= \Phi_0^2 - \frac{h_1}{2}\Phi_1^1 - \frac{h_2}{2}\Phi_1^2 - \left(\frac{h_1}{2}\right)^2\Phi_2^1 + \left(\frac{h_2}{2}\right)^2\Phi_2^2\\ \Phi_0^3 &= \Phi_0^2 + \frac{h_3}{2}\Phi_1^3 + \frac{h_2}{2}\Phi_1^2 - \left(\frac{h_3}{2}\right)^2\Phi_2^3 + \left(\frac{h_2}{2}\right)^2\Phi_2^2\end{aligned} \tag{27}$$

These reduce the unknown electric variables of the vibration problem to,

$$\Phi_0^2, \Phi_1^1, \Phi_1^2, \Phi_1^3, \Phi_2^1, \Phi_2^2, \Phi_2^3 \tag{28}$$

3.1. Equations of motion

The harmonic equations of motion of the piezoelectric sandwich simply-supported plate are obtained from the 2D variational equation (Eq. (18)) by its integration by parts so that virtual variations of the unknowns, Eqs. (23), (26) or (28), appear explicitly. Then, terms multiplying each independent variable are grouped together and made vanish so that the following mechanical equations of motion are obtained,

$$\begin{aligned}
&\delta U^1 : \left(N_{xx}^1 + \frac{1}{2}N_{xx}^2\right)_{,x} + \left(N_{xy}^1 + \frac{1}{2}N_{xy}^2\right)_{,y} - \frac{1}{h_2}(M_{xx,x}^2 + M_{xy,y}^2 - Q_{xz}^2) = \omega^2 J_x^1\\
&\delta V^1 : \left(N_{xy}^1 + \frac{1}{2}N_{xy}^2\right)_{,x} + \left(N_{yy}^1 + \frac{1}{2}N_{yy}^2\right)_{,y} - \frac{1}{h_2}(M_{xy,x}^2 + M_{yy,y}^2 - Q_{yz}^2) = \omega^2 J_y^1\\
&\delta B_x^1 : \left(M_{xx}^1 - \frac{h_1}{2h_2}M_{xx}^2\right)_{,x} + \left(M_{xy}^1 - \frac{h_1}{2h_2}M_{xy}^2\right)_{,y} - \left(Q_{xz}^1 - \frac{h_1}{2h_2}Q_{xz}^2\right) + \frac{h_1}{4}\left(N_{xx,x}^2 + N_{xy,y}^2\right) = \omega^2 \Gamma_x^1\\
&\delta B_y^1 : \left(M_{xy}^1 - \frac{h_1}{2h_2}M_{xy}^2\right)_{,x} + \left(M_{yy}^1 - \frac{h_1}{2h_2}M_{yy}^2\right)_{,y} - \left(Q_{yz}^1 - \frac{h_1}{2h_2}Q_{yz}^2\right) + \frac{h_1}{4}\left(N_{xy,x}^2 + N_{yy,y}^2\right) = \omega^2 \Gamma_y^1\\
&\delta W : (Q_{xz}^1 + Q_{xz}^2 + Q_{xz}^3)_{,x} + (Q_{yz}^1 + Q_{yz}^2 + Q_{yz}^3)_{,y} = \omega^2 J_z^2\\
&\delta U^3 : \left(N_{xx}^3 + \frac{1}{2}N_{xx}^2\right)_{,x} + \left(N_{xy}^3 + \frac{1}{2}N_{xy}^2\right)_{,y} + \frac{1}{h_2}(M_{xx,x}^2 + M_{xy,y}^2 - Q_{xz}^2) = \omega^2 J_x^3\\
&\delta V^3 : \left(N_{xy}^3 + \frac{1}{2}N_{xy}^2\right)_{,x} + \left(N_{yy}^3 + \frac{1}{2}N_{yy}^2\right)_{,y} + \frac{1}{h_2}(M_{xy,x}^2 + M_{yy,y}^2 - Q_{yz}^2) = \omega^2 J_y^3\\
&\delta B_x^3 : \left(M_{xx}^3 - \frac{h_3}{2h_2}M_{xx}^2\right)_{,x} + \left(M_{xy}^3 - \frac{h_3}{2h_2}M_{xy}^2\right)_{,y} - \left(Q_{xz}^3 - \frac{h_3}{2h_2}Q_{xz}^2\right) - \frac{h_3}{4}\left(N_{xx,x}^2 + N_{xy,y}^2\right) = \omega^2 \Gamma_x^3\\
&\delta B_y^3 : \left(M_{xy}^3 - \frac{h_3}{2h_2}M_{xy}^2\right)_{,x} + \left(M_{yy}^3 - \frac{h_3}{2h_2}M_{yy}^2\right)_{,y} - \left(Q_{yz}^3 - \frac{h_3}{2h_2}Q_{yz}^2\right) - \frac{h_3}{4}\left(N_{xy,x}^2 + N_{yy,y}^2\right) = \omega^2 \Gamma_y^3
\end{aligned} \tag{29}$$

where,

$$\begin{aligned}
J_x^1 &= (I_0^1 + I_{11}^2)U^1 + \left(I_1^1 + \frac{h_1}{2}I_{11}^2\right)B_x^1 + I_{13}^2 U^3 - \frac{h_3}{2}I_{13}^2 B_x^3\\
J_x^3 &= (I_0^3 + I_{33}^2)U^3 + \left(I_1^3 - \frac{h_3}{2}I_{33}^2\right)B_x^3 + I_{13}^2 U^1 + \frac{h_1}{2}I_{13}^2 B_x^1, \quad J_z^2 = (I_0^1 + I_0^2 + I_0^3)W\\
\Gamma_x^1 &= \left(I_1^1 + \frac{h_1}{2}I_{11}^2\right)U^1 + \left[I_2^1 + \left(\frac{h_1}{2}\right)^2 I_{11}^2\right]B_x^1 + \frac{h_1}{2}I_{13}^2 U^3 - \frac{h_1 h_3}{4}I_{13}^2 B_x^3\\
\Gamma_x^3 &= \left(I_1^3 - \frac{h_3}{2}I_{33}^2\right)U^3 + \left[I_2^3 + \left(\frac{h_3}{2}\right)^2 I_{33}^2\right]B_x^3 - \frac{h_3}{2}I_{13}^2 U^1 - \frac{h_1 h_3}{4}I_{13}^2 B_x^1
\end{aligned}$$

with

$$I_{11}^2 = \frac{I_0^2}{4} - \frac{I_1^2}{h_2} + \frac{I_2^2}{(h_2)^2}, \quad I_{13}^2 = \frac{I_0^2}{4} - \frac{I_2^2}{(h_2)^2}, \quad I_{33}^2 = \frac{I_0^2}{4} + \frac{I_1^2}{h_2} + \frac{I_2^2}{(h_2)^2}$$

The corresponding y-components of J and Γ terms have the same expressions as the previous x-components but with V and B_y instead of U and B_x variables.

The electric equations of motion can be obtained after grouping, then vanishing the terms multiplying virtual variations of electric unknowns. Therefore, they depend on the electric upper and lower faces electric boundary conditions. Hence, for short-circuited plate electrodes, the following equations hold for the electric variables of Eq. (26),

$$\begin{aligned}
&\delta\Phi_1^1 : \widetilde{D}_{x,x}^{12} + \widetilde{D}_{y,y}^{12} + \left(\overline{D}_{0z}^1 - \frac{h_1}{h_2}\overline{D}_{0z}^2\right) = 0\\
&\delta\Phi_1^3 : \widetilde{D}_{x,x}^{32} + \widetilde{D}_{y,y}^{32} + \left(\overline{D}_{0z}^3 - \frac{h_3}{h_2}\overline{D}_{0z}^2\right) = 0\\
&\delta\Phi_2^1 : \breve{D}_{x,x}^1 + \breve{D}_{y,y}^1 + 2\overline{D}_{1z}^1 = 0\\
&\delta\Phi_2^2 : \breve{D}_{x,x}^2 + \breve{D}_{y,y}^2 + 2\overline{D}_{1z}^2 = 0\\
&\delta\Phi_2^3 : \breve{D}_{x,x}^3 + \breve{D}_{y,y}^3 + 2\overline{D}_{1z}^3 = 0
\end{aligned} \tag{30}$$

where,

$$\widetilde{D}_\alpha^{12} = -\frac{h_1}{2}(\overline{D}_{0\alpha}^1 + \overline{D}_{0\alpha}^2) - \left(\overline{D}_{1\alpha}^1 - \frac{h_1}{h_2}\overline{D}_{1\alpha}^2\right)$$

$$\widetilde{D}_\alpha^{32} = \frac{h_3}{2}(\overline{D}_{0\alpha}^3 + \overline{D}_{0\alpha}^2) - \left(\overline{D}_{1\alpha}^3 - \frac{h_3}{h_2}\overline{D}_{1\alpha}^2\right), \quad \breve{D}_\alpha^k = \left(\frac{h_k}{2}\right)^2 \overline{D}_{0\alpha}^k - \overline{D}_{2\alpha}^k$$

Similar notations are used for open-circuited upper and lower face plate electrodes,

$$\hat{D}_\alpha = \overline{D}_{0\alpha}^1 + \overline{D}_{0\alpha}^2 + \overline{D}_{0\alpha}^3, \quad \widetilde{D}_\alpha = \frac{h_2}{2}(\overline{D}_{0\alpha}^1 - \overline{D}_{0\alpha}^3) - \overline{D}_{1\alpha}^2, \quad \breve{D}_\alpha = -\left(\frac{h_2}{2}\right)^2 (\overline{D}_{0\alpha}^1 + \overline{D}_{0\alpha}^3) - \overline{D}_{2\alpha}^2$$

$$\widetilde{D}_\alpha^1 = \frac{h_1}{2}\overline{D}_{0\alpha}^1 - \overline{D}_{1\alpha}^1, \quad \breve{D}_\alpha^1 = \left(\frac{h_1}{2}\right)^2 \overline{D}_{0\alpha}^1 - \overline{D}_{2\alpha}^1$$

$$\widetilde{D}_\alpha^3 = -\frac{h_3}{2}\overline{D}_{0\alpha}^3 - \overline{D}_{1\alpha}^3, \quad \breve{D}_\alpha^3 = \left(\frac{h_3}{2}\right)^2 \overline{D}_{0\alpha}^3 - \overline{D}_{2\alpha}^3$$

so that the corresponding equations to the electric potential variables of Eq. (28) are,

$$
\begin{aligned}
&\delta\Phi_0^2 : \hat{D}_{x,x} + \hat{D}_{y,y} = 0\\
&\delta\Phi_1^1 : \widetilde{D}_{x,x}^1 + \widetilde{D}_{y,y}^1 + \overline{D}_{0z}^1 = 0\\
&\delta\Phi_1^2 : \widetilde{D}_{x,x} + \widetilde{D}_{y,y} + \overline{D}_{0z}^2 = 0\\
&\delta\Phi_1^3 : \widetilde{D}_{x,x}^3 + \widetilde{D}_{y,y}^3 + \overline{D}_{0z}^3 = 0\\
&\delta\Phi_2^1 : \breve{D}_{x,x}^1 + \breve{D}_{y,y}^1 + 2\overline{D}_{1z}^1 = 0\\
&\delta\Phi_2^2 : \breve{D}_{x,x} + \breve{D}_{y,y} + 2\overline{D}_{1z}^2 = 0\\
&\delta\Phi_2^3 : \breve{D}_{x,x}^3 + \breve{D}_{y,y}^3 + 2\overline{D}_{1z}^3 = 0
\end{aligned}
\tag{31}
$$

It is worthy to notice that although mechanical (29) and electric (30) or (31) equations of motion appear uncoupled, the electromechanical coupling is in fact present implicitly through the generalized piezoelectric constitutive equations (Eqs. (19a), (19b), (20a) and (20b)).

3.2. Free-vibrations problem

The generalized constitutive equations (Eqs. (19a), (19b), (20a) and (20b)) are to be expressed in terms of the mechanical (23) and electric (26) or (28) unknown variables, then substituted into the mechanical (29) and electric (30) or (31) equations of motion. Therefore, the harmonic vibration problem in hand reduces to the solution of the following linear generalized eigenvalue problem,

$$
(\mathbf{K}^* - \omega^2\mathbf{M}^*)\overset{*}{\underset{\sim}{\mathbf{U}}} = \underset{\sim}{\mathbf{0}} \tag{32}
$$

where $\mathbf{K}^*$ and $\mathbf{M}^*$ are the stiffness and mass matrices. $\overset{*}{\underset{\sim}{\mathbf{U}}}$ is the vector of mechanical and electric unknowns.

The linear system of Eq. (32) is of order 14 or 16 depending on the considered electric boundary conditions on upper and lower electrodes. Therefore, to get a unified eigenvalue problem, the above system is splitted into mechanical and electric separate contributions,

$$
\left(\begin{bmatrix} \mathbf{K}_{UU} & \mathbf{K}_{U\Phi} \\ \mathbf{K}_{\Phi U} & \mathbf{K}_{\Phi\Phi} \end{bmatrix} - \omega^2 \begin{bmatrix} \mathbf{M}_{UU} & \mathbf{0} \\ \mathbf{0} & \mathbf{0} \end{bmatrix}\right) \begin{Bmatrix} \underset{\sim}{\mathbf{U}} \\ \underset{\sim}{\mathbf{\Phi}} \end{Bmatrix} = \begin{Bmatrix} \underset{\sim}{\mathbf{0}} \\ \underset{\sim}{\mathbf{0}} \end{Bmatrix} \tag{33}
$$

so that the electric unknowns can be obtained from its second bloc line by,

$$
\underset{\sim}{\mathbf{\Phi}} = -\mathbf{K}_{\Phi\Phi}^{-1}\mathbf{K}_{\Phi U}\underset{\sim}{\mathbf{U}} \tag{34}
$$

Substituting this result into the first line of Eq. (33), leads to the following reduced system,

$$
(\mathbf{K} - \omega^2\mathbf{M})\underset{\sim}{\mathbf{U}} = \underset{\sim}{\mathbf{0}} \tag{35}
$$

with

$$
\mathbf{K} = \mathbf{K}_{UU} - \mathbf{K}_{U\Phi}\mathbf{K}_{\Phi\Phi}^{-1}\mathbf{K}_{\Phi U}; \quad \mathbf{M} = \mathbf{M}_{UU}
$$

The latter reduced system is first solved to obtain the eigen frequencies and corresponding mechanical constants, then the electric ones are computed a posteriori using Eq. (34).

4. Numerical validation and analysis

The present 2D closed-form solution has been derived partially using the symbolic software Maple®, combined with Matlab® for its numerical implementation. To validate the present approach, single- and three-layer piezoelectric, and hybrid sandwich plates, with side length $L_x = L_y = a$ and total thickness $h = 0.01$ m, are analyzed. Computed modal characteristics are compared to those obtained with the 3D exact solution of Heyliger and Saravanos (1995) for $m_x = m_y = 1$, and with the mixed FSDT/layerwise finite element (FE) one of Correia et al. (2000) for various (m_x, m_y) couples. Material properties are those given in the former reference. In particular, a unit mass density is retained for comparison purpose.

4.1. Single-layer piezoelectric plate

This sub-section aims to check the correct degeneration of the present sandwich formulation to a single-layer one and to study the influence of the electric boundary conditions and the plate thickness ratio a/h on the plate piezoelectric behavior. A simply-supported square piezoceramic (PZT-4) plate with variable thickness ratio, and either short-($\Phi = 0$) or open-($D_z = 0$) circuited is then considered. The thickness of each face is made vanish so that the present sandwich formulation reduces to a classical single-layer first-order shear deformation one.

Results of the first three modes for $m_x = m_y = 1$ are compared, in Table 1, to those obtained by Heyliger and Saravanos (1995) using a 3D exact solution. An excellent agreement between present and reference results is obtained even for the thick plate ($a/h = 4$), although the Mindlin-type formulation is known to be suited mainly for relatively thick plates ($a/h = 10$). Present results were obtained without use of the shear correction factor required by FSDT. In fact, it was found that the plate frequencies did not vary much with the shear correction factor value. The good results shown in Table 1 prove the correct degeneration of the sandwich formulation to the single-layer one, obtained by vanishing each face thickness. Table 1 indicates that the open-circuit electric boundary condition provides higher frequencies than the short-circuit case, except for the second mode which is an uncoupled membrane one. Also, it is clear from Table 1 that the precision of the present closed solution augments with the thickness ratio a/h.

4.2. Piezoelectric sandwich plate

To validate the sandwich aspect of the present closed-form 2D solution, a square piezoelectric three-layer plate, with thickness ratios $a/h = 4$ (thick) and $a/h = 50$ (thin) and either short- or open-circuited on

Table 1
First three circular frequencies ($\omega/100$ rad/s) for $m_x = m_y = 1$ of a square PZT-4 plate

a/h	Exact 3D layerwise solution Heyliger and Saravanos (1995)		Present 2D sandwich solution		Error (%) = 100(2D − 3D)/3D	
	$\Phi = 0$	$D_z = 0$	$\Phi = 0$	$D_z = 0$	$\Phi = 0$	$D_z = 0$
4	96929.9	98231.7	98246.6	99634.9	1.36	1.43
	194255	194255	194255.2	194255.2	0	0
	327663	355110	335395.8	361925.6	2.36	1.92
10	18013.4	18077.8	18071.1	18136.4	0.32	0.32
	77702.1	77702.1	77702.1	77702.1	0	0
	133695	145221	134158.3	145609.7	0.35	0.27
50	746.752	746.873	746.837	746.957	0.01	0.01
	15540.4	15540.4	15540.4	15540.4	0	0
	26828	29153.3	26831.7	29155.6	0.01	0.01

its upper and lower surfaces, is analyzed for two configurations: (i) PVDF/PZT-4/PVDF: the plate has piezoelectric polymeric soft faces and piezoceramic rigid core; (ii) PZT-4/PVDF/PZT-4: the plate has piezoceramic rigid faces and piezoelectric polymeric soft core. For both configurations, the core is twice thicker than each face. 3D exact results of Heyliger and Saravanos (1995) are taken as references for the first five modes (Table 2).

As expected, the present approach is found to be more accurate for the sandwich configuration (ii) with soft core and rigid faces. This is due to the well representation, by the present approach, of the additional shear induced by the sliding of the rigid faces (PZT-4) against the soft core (PVDF). However, in the opposite configuration (i) and for higher modes than 3, where the transverse shear is more present, the polymeric soft faces are unable to shear the piezoceramic rigid core. The present approach is also less accurate for thick ($a/h = 4$) configurations. This is inherent to the first-order shear deformation theories which are in general accurate for $a/h \geqslant 10$. Displacements and electric potential are normalized by their respective maximum values and represented in Figs. 2 and 3 for short-circuited configurations (i) and (ii), respectively. They show exact electric potential distribution for both ratios and exact displacement ones for the thin case only. However, linear, instead of quadratic, in-plane displacements and constant, instead of linear, deflection (Heyliger and Saravanos, 1995) are obtained in PVDF layers for thick plates.

4.3. Hybrid piezoelectric–elastic sandwich plate

A more realistic adaptive sandwich plate configuration, than previous examples, is now considered. It consists of a symmetric equal-thickness three-layer cross-ply (0°/90°/0°) graphite/epoxy laminate core

Table 2
First five circular frequencies ($\omega/100$ rad/s) for $m_x = m_y = 1$ of a square piezoelectric sandwich plate

Sandwich scheme	a/h	Exact 3D layerwise solution Heyliger and Saravanos (1995)		Present 2D sandwich solution		Error (%) = 100(2D − 3D)/3D	
		$\Phi = 0$	$D_z = 0$	$\Phi = 0$	$D_z = 0$	$\Phi = 0$	$D_z = 0$
(i) Configuration PVDF/ PZT-4/PVDF	4	72174.4	72191.5	73969.5	74006	2.49	2.51
		194760	194881	197165	197279.6	1.24	1.23
		306209	306539	329399.5	329861.6	7.57	7.61
		337107	337196	345026.8	345226	2.35	2.38
		424602	424664	459653.3	459693.3	8.26	8.25
	50	633.417	633.487	633.666	633.735	0.04	0.04
		16431.1	16440.9	16432.5	16442.3	0.01	0.01
		28535.2	28555.3	28537.6	28557.7	0.01	0.01
		268118	271222	292031.9	295866.2	8.92	9.09
		353079	362248	379316.5	390810.4	7.43	7.89
(ii) Configuration PZT-4/ PVDF/ PZT-4	4	58248.7	58354	58339.5	58445.4	0.16	0.15
		192408	192436	204629.8	204650	6.35	6.35
		271757	271758	275428.9	275429.3	1.35	1.35
		329584	329593	355778.2	356148.2	7.95	8.06
		363048	364072	413006.4	414334.3	13.8	13.8
	50	725.219	725.241	725.230	725.252	0	0
		16430.2	16438.8	16436.9	16445.6	0.04	0.04
		28535.7	28555.1	28540.4	28559.9	0.02	0.02
		159732	159865	161063.6	161204.3	0.83	0.84
		226218	226643	228455.9	228903.6	0.99	1.0

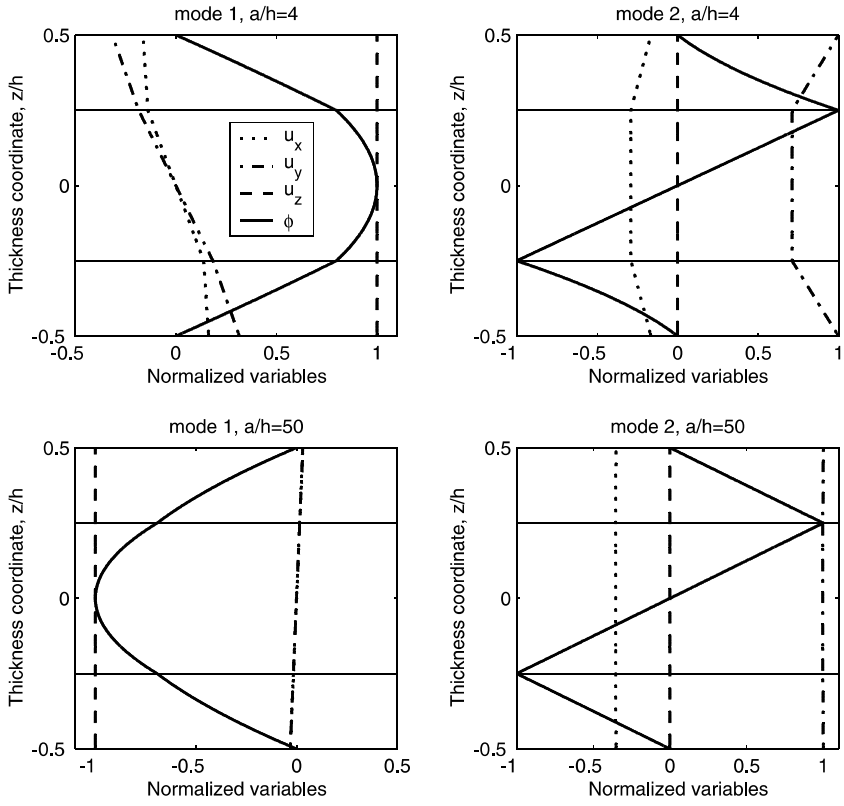

Fig. 2. Normalized displacement and electric potential through-thickness variations for the first two modes of a short-circuited PVDF/PZT-4/PVDF sandwich simply-supported square plate.

sandwiched between two $0.1h$-thick piezoceramic (PZT-4) faces. The composite core material properties are homogenized from those of Heyliger and Saravanos (1995). Circular frequencies, for $m_x = m_y = 1$, are evaluated with the present approach for both short- and open-circuit electric boundary conditions on upper and lower faces, and for two thickness ratios of the hybrid plate.

The calculated first four circular frequencies are compared in Table 3 to 3D exact ones (Heyliger and Saravanos, 1995). It is clear that they agree very well with the reference values, in particular for the thin plate case ($a/h = 50$). In the latter case, the difference between short- and open-circuit frequencies tend to vanish.

The present 2D sandwich closed-form solution is now used to show its utility as a reference for 2D FE solutions. Hence, for both boundary conditions and both thickness ratios, the first five frequency parameters, $\lambda = \omega a^2 \rho^{1/2}/(2\pi h)$, of the hybrid plate, calculated with a mixed FSDT (for mechanical behavior) and linear layerwise (for electric behavior) FE approach (Correia et al., 2000), are compared to those obtained by the present closed solution (Table 4). It was found that the FE values correspond to the first frequencies of fixed couples (m_x, m_y). The fundamental frequencies ($m_x = m_y = 1$) are also compared to the 3D exact ones of Heyliger and Saravanos (1995) and to the full linear layerwise FE results (with constant deflection) of Saravanos et al. (1997).

Table 4 indicates that the analytical frequencies do not depend much on the electric boundary conditions. This dependence is therefore much higher for FE results. Those of Correia et al. (2000) agree well with the analytical ones for the open-circuit electric boundary condition and thin plate case only. Higher

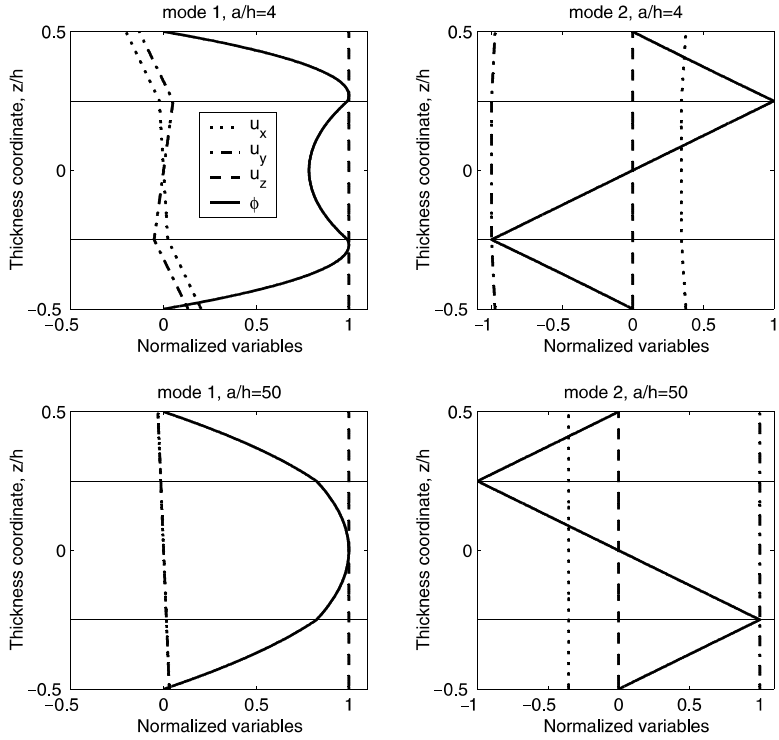

Fig. 3. Normalized displacement and electric potential through-thickness variations for the first two modes of a short-circuited PZT-4/PVDF/PZT-4 sandwich simply-supported square plate.

Table 3
First four thickness ($m_x = m_y = 1$) circular frequencies ($\omega/100$ rad/s) of a square hybrid sandwich plate

a/h	Exact 3D layerwise solution Heyliger and Saravanos (1995)		Present 2D sandwich solution		Error (%) $= 100(2D - 3D)/3D$	
	$\Phi = 0$	$D_z = 0$	$\Phi = 0$	$D_z = 0$	$\Phi = 0$	$D_z = 0$
4	57074.5	57089.3	58216.1	58231	2.0	2.0
	191301	191304	196017.7	196019.9	2.47	2.47
	250769	250770	268650	268650.2	7.13	7.13
	274941	274941	283754.1	283754.1	3.21	3.21
50	618.118	618.120	618.435	618.437	0.05	0.05
	15681.6	15681	15684	15684	0.02	0.02
	21492.8	21493	21499.4	21499.6	0.03	0.03
	209704	209707	214834	214865.6	2.45	2.46

discrepancies appear for the corresponding short-circuited condition, in particular for the fundamental mode, which does not correspond to neither FE layerwise nor present analytic solutions. This may be due to nil in-plane electric field and displacement assumptions retained in Correia et al. (2000), but not considered in the other two solutions. Higher errors for the thin plate case may also be due to possible shear locking of the FSDT element. Notice also that for the thick plate case, a double-frequency mode was obtained by Correia et al. (2000). However, the presence of this mode is not confirmed by the visualization of the six first modes of the short-circuited thick hybrid plate given by the present closed solution (Fig. 4).

Table 4
First five frequency parameters, $\lambda = \omega a^2 \rho^{1/2}/(2\pi h)$ (10^3 Hz (kg/m)$^{1/2}$), of a square hybrid sandwich plate

a/h	m_x	m_y	Present 2D sandwich solution (ref.)		2D FE solution (Q9-FSDT 5P) Correia et al. (2000)		Error (%) = 100(FE − ref.)/ref.	
			$\Phi = 0$	$D_z = 0$	$\Phi = 0$	$D_z = 0$	$\Phi = 0$	$D_z = 0$
4	1	1	148.246	148.283	142.068	147.489	−4.17	−0.54
			145.339[a]	145.377[a]	145.323[b]	151.222[b]		
	–	–	–	–	206.304	206.304	–	–
	–	–	–	–	206.304	206.304	–	–
	1	2	261.212	261.335	259.586	265.931	−0.62	1.76
	2	1	275.112	275.205	276.536	280.328	0.59	1.86
	2	2	353.957	354.151	–	–	–	–
	1	3	391.924	392.191	–	–	–	–
50	1	1	246.067	246.068	206.304	245.349	−16.16	−0.29
			245.941[a]	245.942[a]	236.833[b]	259.173[b]		
	1	2	559.615	559.621	519.444	558.988	−7.18	−0.11
	2	1	693.601	693.606	663.336	694.196	−4.36	0.08
	2	2	967.141	967.155	907.636	962.017	−6.15	−0.53
	1	3	1091.458	1091.481	1020.102	1093.006	−6.54	0.14

[a] 3D layerwise exact solution (Heyliger and Saravanos, 1995).
[b] 2D layerwise FE solution (w-constant) (Saravanos et al., 1997).

5. Thickness modes analysis of a hybrid sandwich plate

After its validation, the present formulation is now used to analyze the thickness modes ($m_x = m_y = 1$) of the square short-circuited hybrid sandwich plate used in the previous sub-section. The same piezoelectric and elastic material properties are also retained here. Therefore, the plate has now in-plane dimensions $L_x = L_y = a = 10h$ and true mass densities of PZT-4 (7600 kg/m^3) and graphite/epoxy (1578 kg/m^3) materials. For each mode, modal shape, and through-thickness variations of the displacements and electric potential are represented and commented.

5.1. First mode

The first mode of the hybrid sandwich plate is a pure bending one as shown in Fig. 5a. Through-thickness variations of its displacement components (Fig. 5b) indicate that it can be well represented by a unique displacement field as used in the classical ESL theory. That is, the in-plane components are through-thickness linear and nil at the mid-plane $z = 0$; whereas, the transverse deflection is constant. The electric potential is linear in the piezoelectric faces and almost constant in the elastic core (Fig. 5b). Therefore, this mode needs layerwise electric potential for its good representation. Its electromechanical behavior can then be modeled by a mixed ESL/layerwise approach.

5.2. Second mode

The second mode of the hybrid sandwich plate is a membrane one as can be seen from its modal shape (Fig. 6a). Through-thickness displacement variations (Fig. 6b) confirm this conclusion since the in-plane components are constant and the transverse one is nil. Here, the electric potential is piecewise linear through the plate thickness. Thus, this mode can also be well represented by a mixed ESL/layerwise model.

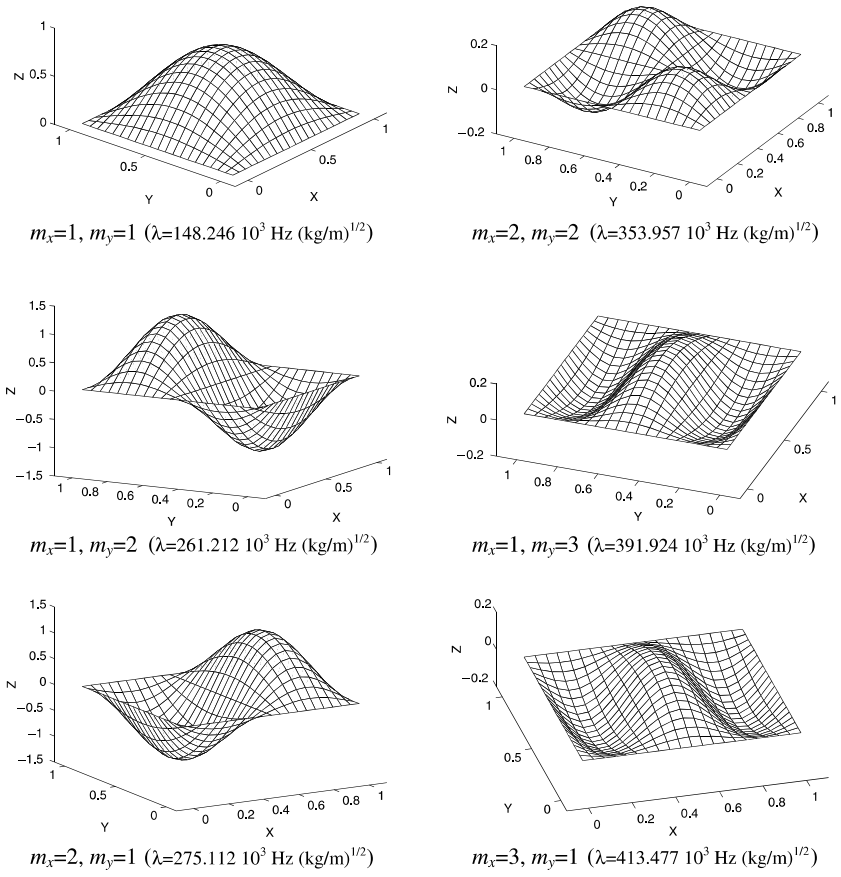

Fig. 4. First six modes of short-circuited hybrid sandwich simply-supported square plate ($a/h = 4$).

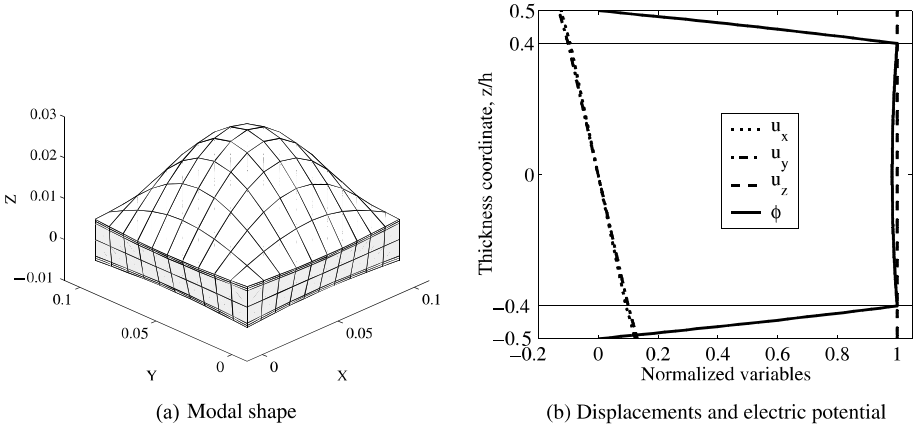

(a) Modal shape (b) Displacements and electric potential

Fig. 5. The first thickness ($m_x = m_y = 1$) mode of the short-circuited hybrid sandwich plate.

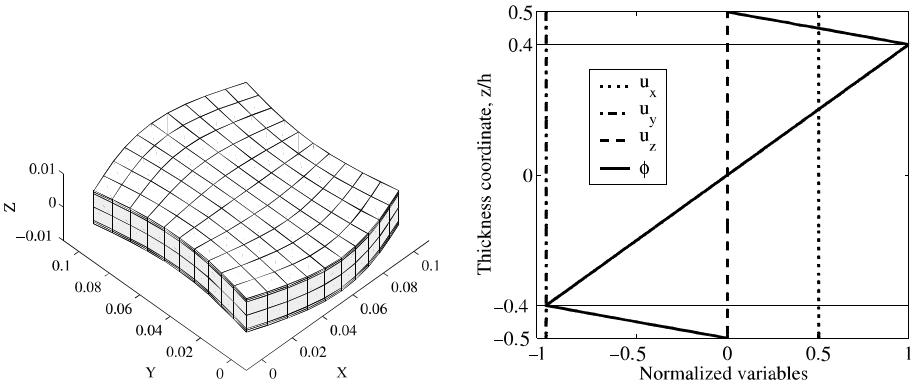

(a) Modal shape (b) Displacements and electric potential

Fig. 6. The second thickness ($m_x = m_y = 1$) mode of the short-circuited hybrid sandwich plate.

5.3. Third mode

The third mode, shown in Fig. 7a, is also a membrane one. However, compared to the second mode, Fig. 7b indicates that the present one is dominated by the u_x displacement instead of u_y. It has similar electric potential distribution but in opposite sign. This mode can also be well represented by a mixed ESL/layerwise model.

5.4. Fourth mode

The modal shape of the fourth mode is presented in Fig. 8a. Its in-plane displacements are linear in the elastic core and constant in the piezoceramic faces, whereas, the transverse defection is almost nil (Fig. 8b). The electric potential has the same through-thickness distribution as the first mode. Thus, this mode can not be well represented by a mixed ESL/layerwise model. Fig. 8a shows clearly the shear of the core by the faces. Hence, this mode is the first transverse shear mode characterized by the relative displacements of the faces with respect to the core.

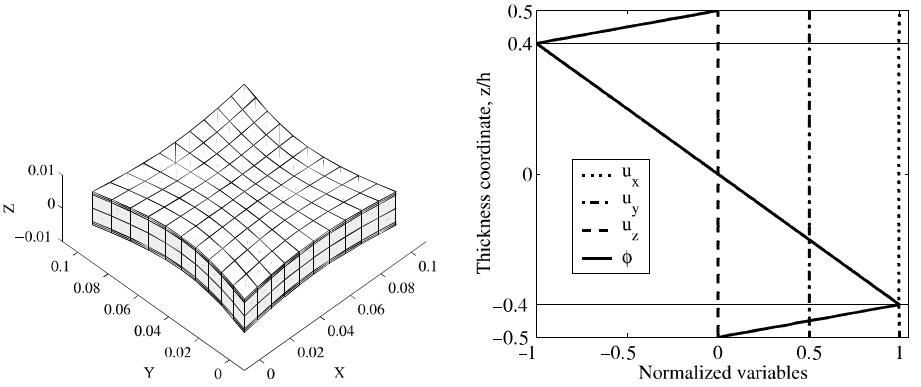

(a) Modal shape (b) Displacements and electric potential

Fig. 7. The third thickness ($m_x = m_y = 1$) mode of the short-circuited hybrid sandwich plate.

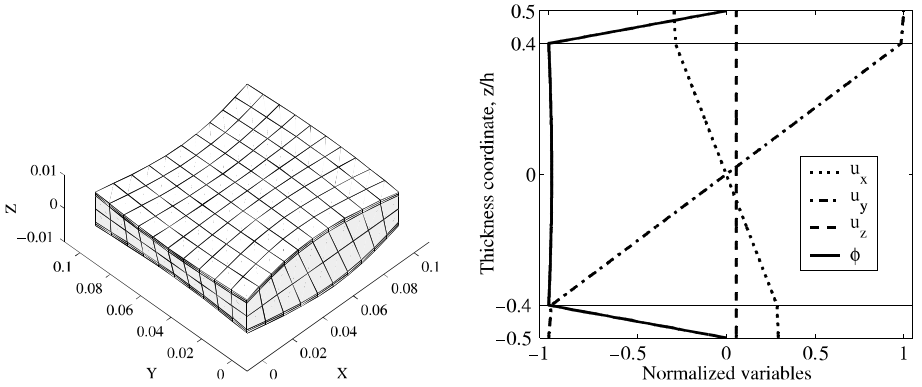

(a) Modal shape (b) Displacements and electric potential

Fig. 8. The fourth thickness ($m_x = m_y = 1$) mode of the short-circuited hybrid sandwich plate.

5.5. Fifth mode

The modal shape of the fifth mode is shown in Fig. 9a. Here, as for the second and third modes, the in-plane displacement components interchange their roles compared to the previous mode, whereas the electric potential keeps the same distribution (Fig. 9b). This mode can then be interpreted as the second transverse shear mode. Notice that the present and previous modes are dominated by the deformation of the core, whereas, the first three modes are global; i.e. the plate deforms in a whole. Fig. 9b also indicates that this mode is characteristic of the sandwich behavior, thus cannot be well represented using a mixed ESL/layerwise theory.

5.6. Sixth mode

The sixth mode is represented in Fig. 10a. The latter indicates that there is a relative rotation of the faces against the core, which has a membrane behavior. This is confirmed by Fig. 10b, showing that the in-plane displacements have opposite signs with linear and constant variations in the faces and the core, respectively. The transverse deflection of the whole plate is nil. Electrically, the mode has linear and slightly quadratic

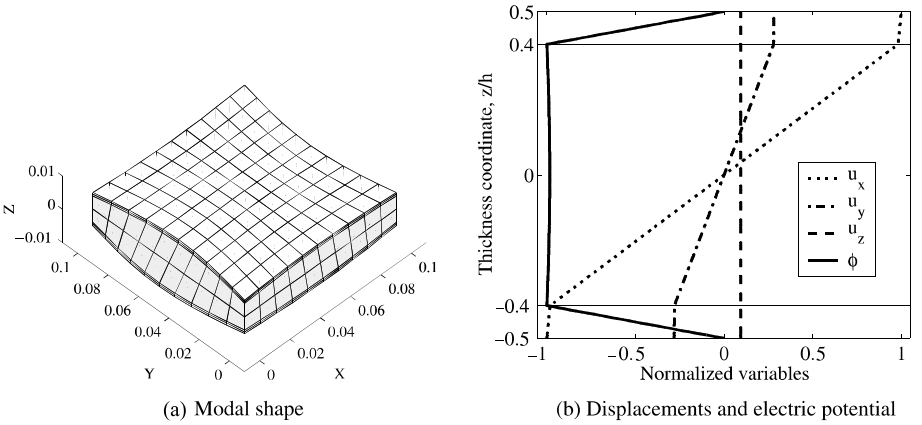

(a) Modal shape (b) Displacements and electric potential

Fig. 9. The fifth thickness ($m_x = m_y = 1$) mode of the short-circuited hybrid sandwich plate.

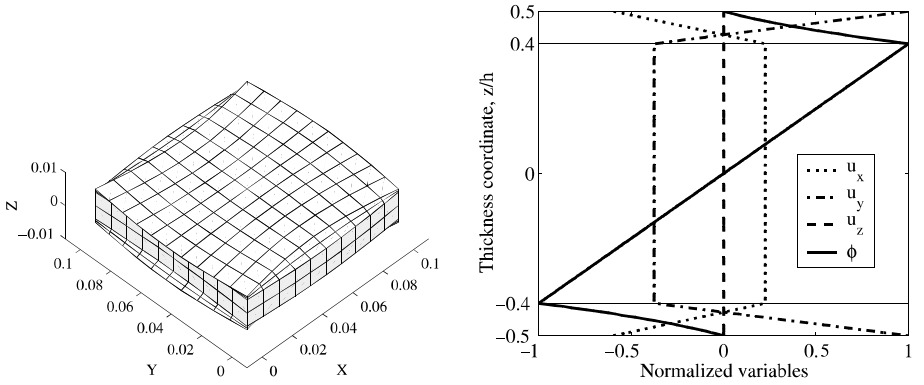

(a) Modal shape (b) Displacements and electric potential

Fig. 10. The sixth thickness ($m_x = m_y = 1$) mode of the short-circuited hybrid sandwich plate.

electric potentials in the elastic composite core and piezoceramic faces, respectively. Again, this mode cannot be obtained using a mixed ESL/layerwise method. Notice, that compared to the previous fourth and fifth modes, the present one is dominated by the deformations of the faces.

5.7. Seventh mode

As for the previous mode, the seventh, represented in Fig. 11a, is dominated by the faces deformations. Fig. 11b confirms this conclusion and shows that, in contrary to the sixth mode, the present one has identical in-plane displacements signs. Its electric potential has the same distribution through the plate thickness. This mode can then be well represented only by a layerwise electromechanical model. It is worthy to notice that it has almost the same frequency (0.05% relative difference) as the sixth mode.

5.8. Eighth mode

The modal shape of this mode, represented in Fig. 12a, is also dominated by the faces deformations. However, in comparison with the last two modes, here the core bends (Fig. 12b). Electrically, the present

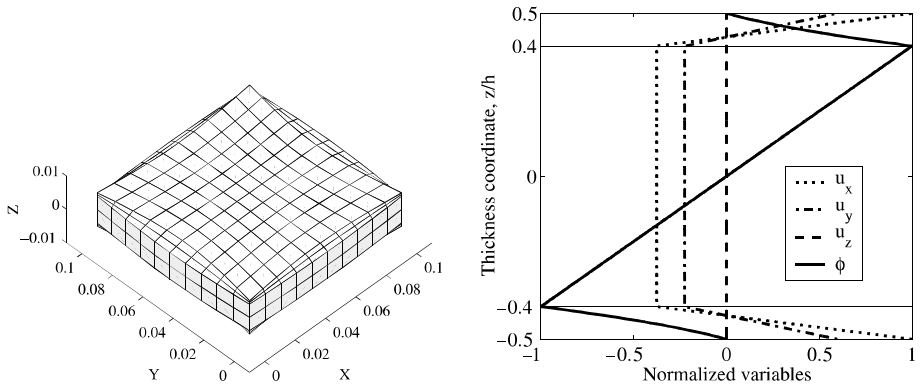

(a) Modal shape (b) Displacements and electric potential

Fig. 11. The seventh thickness ($m_x = m_y = 1$) mode of the short-circuited hybrid sandwich plate.

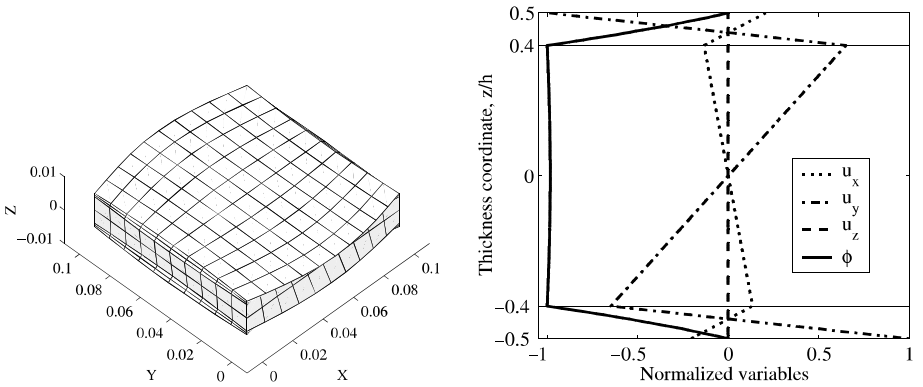

(a) Modal shape (b) Displacements and electric potential

Fig. 12. The eighth thickness ($m_x = m_y = 1$) mode of the short-circuited hybrid sandwich plate.

mode has slight quadratic potentials in the piezoelectric faces and nearly constant one in the elastic composite core. It is clear also, from Fig. 12b, that this mode can be well represented only using an electromechanical full layerwise model.

5.9. Ninth mode

This mode, represented in Fig. 13a, has almost the same frequency (0.1% relative difference) and electric distribution (Fig. 13b) as the previous one, but with in-plane displacement roles that interchange. Again, due to the full layerwise variations of the displacements and electric potential, this mode will not be well represented using a ESL/layerwise model.

The previous detailed analysis of the nine thickness modes of the adaptive sandwich plate has shown that the six last modes, characteristic of its sandwich behavior, are dominated by the displacements of either the core (fourth and fifth modes) or the faces (sixth to ninth modes). To check this result, the following mean (barred) and relative (waved) generalized displacements of the faces, augmented by the deflection W, are defined from Eqs. (22) and (23),

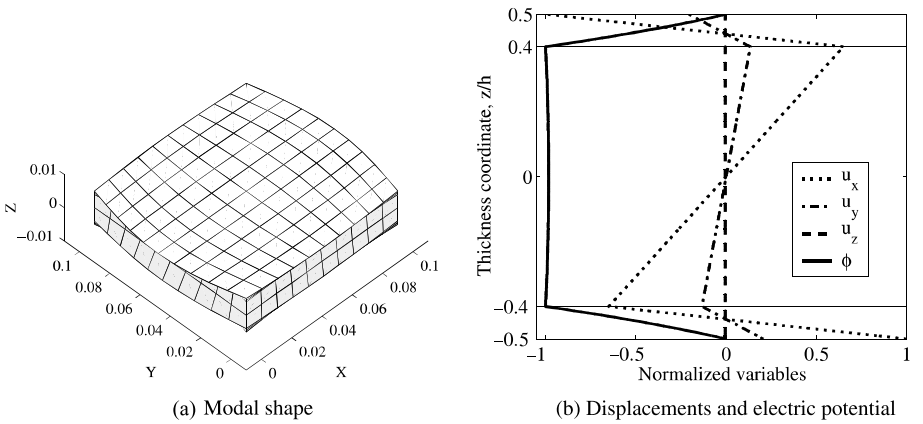

(a) Modal shape (b) Displacements and electric potential

Fig. 13. The ninth thickness ($m_x = m_y = 1$) mode of the short-circuited hybrid sandwich plate.

Table 5
Normalized mean and relative displacements for the thickness modes of the adaptive sandwich plate

Modes	1	2	3	4	5	6	7	8	9
$\overline{U}$	0	*0.1518*	*0.1583*	0	0	−0.0001	0.0001	0	0
$\overline{V}$	0	*−0.3008*	*0.0798*	0	0	0.0001	0.0001	0	0
W	*0.0322*	0	0	0.0039	0.0051	0	0	0	0
$\overline{B}_x$	*−1*	0	0	*−0.5249*	*1*	0	0	*0.2067*	*−1*
$\overline{B}_y$	*−0.9997*	0	0	*1*	*0.1068*	0	0	*−1*	*−0.2067*
$\widetilde{U}$	−0.0070	0	0	*−0.0396*	*0.1077*	0	0	0	*−0.0002*
$\widetilde{V}$	−0.0075	0	0	*0.1355*	*0.0305*	0	0	−0.0002	0
$\widetilde{B}_x$	0	*1*	*1*	0	0	*−0.5975*	1	0	0
$\widetilde{B}_y$	0	*−0.9020*	*0.2169*	0	0	1	*0.5975*	0	0

$$\begin{aligned} &\overline{U} = \tfrac{1}{2}(U^3 + U^1), \quad \overline{V} = \tfrac{1}{2}(V^3 + V^1), \quad \overline{B}_x = \tfrac{1}{2}(B_x^3 + B_x^1), \quad \overline{B}_y = \tfrac{1}{2}(B_y^3 + B_y^3), \quad W \\ &\widetilde{U} = U^3 - U^1, \quad \widetilde{V} = V^3 - V^1, \quad \widetilde{B}_x = B_x^3 - B_x^1, \quad \widetilde{B}_y = B_y^3 - B_y^1 \end{aligned} \tag{36}$$

and analyzed for the nine thickness modes. To identify the dominant variables of each mode, they are normalized with respect to their maximum value and shown in Table 5. The latter confirms the observations made in the previous analysis and shows that:

- The bending mode is dominated by the *mean rotations* and *deflection*,
- The membrane modes are dominated by the *mean in-plane displacements* and *relative rotations*,
- The core sandwich modes (fourth and fifth modes) are dominated by the *relative in-plane displacements* and *mean rotations*,
- The face sandwich modes (sixth to ninth modes) are dominated by either the *relative* (sixth and seventh modes) or the *mean* (eighth and ninth modes) *rotations*.

It is worthy to notice that for thin faces, for which the transverse shear effect can be neglected, the relative rotations vanish and the mean ones will equal the deflection first derivatives. Hence, the above nine fundamental variables, Eq. (36), will reduce to the following five ones only,

$$\overline{U}, \overline{V}, W, \widetilde{U}, \widetilde{V} \tag{37}$$

Therefore there will be only five thickness modes for fixed in-plane mode indices. The present sandwich formulation is very suited for this particular case. In fact, the first five modes described in this analysis are exactly, within a maximum error of 3%, the first five thickness modes given by a specially implemented 3D state space method (Table 6).

The slight augmentation of the percent difference for the last two modes of Table 6 can be due to the homogenization of the material properties of the three-layer composite core. This is confirmed by Fig. 14 showing the 3D through-thickness distributions of the mechanical displacements and electric potential. The

Table 6
First five frequency parameters, $\lambda = \omega a^2 \rho^{1/2}/(2\pi h)$ (10^3 Hz (kg/m)$^{1/2}$), of a square hybrid sandwich plate ($\Phi = 0$, $a/h = 10$, $\rho = \rho_i h_i/h$, $m_x = m_y = 1$)

Exact 3D state space solution	Present 2D sandwich solution	Error (%) = 100(2D − 3D)/3D
214.933	216.602	0.78
1231.799	1247.893	1.31
1702.970	1710.501	0.44
2918.609	2967.704	1.68
3293.101	3392.704	3.02

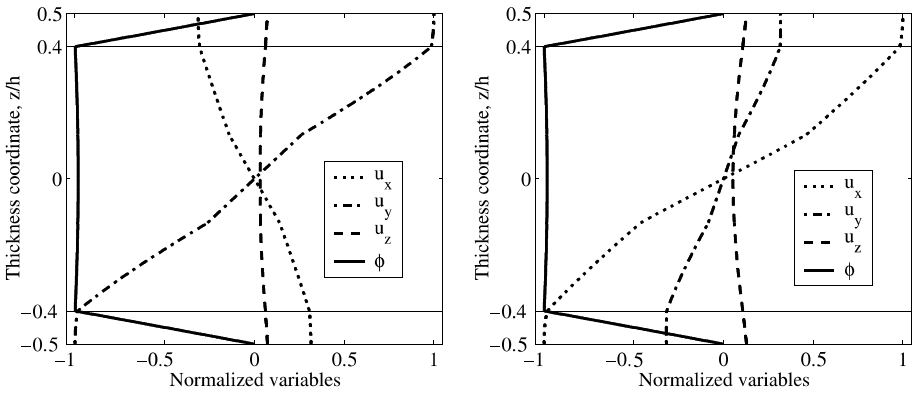

Fig. 14. Displacements and electric potential 3D through-thickness distributions of the (a) fourth and (b) fifth thickness modes of a relatively thick ($a/h = 10$) SC ($\Phi = 0$) adaptive sandwich simply-supported plate.

in-plane displacements are slightly piecewise linear through the composite core, instead of being only linear as retained in the present 2D formulation. Fig. 14 is to be compared to Figs. 8b and 9b. These indicate evidently the good approximations of the in-plane displacements by the present 2D sandwich formulation compared to the exact 3D solution.

6. Conclusions

A 2D closed-form solution for the free-vibrations analysis of simply supported piezoelectric sandwich plates has been presented and validated. It has the originality to consider a quadratic electric potential and FSDT for each layer. Also, no simplifying assumptions were made regarding the in-plane electric field and displacement components. Hence, the electric charge equation was exactly satisfied. Generalized piezoelectric constitutive equations for the introduced stress and electric displacement resultants and 2D mechanical and electric equations of motion of the piezoelectric-adaptive sandwich plate were also derived for the first time. After its validation on single- and three-layer piezoelectric, and hybrid configurations, the present approach has been used to explore the thickness modes of a square relatively thick sandwich plate with piezoelectric faces and symmetric cross-ply graphite/epoxy composite laminate core. From this modal analysis, it was found that:

1. Only the first three modes were global so that the plate deforms in a whole. The remaining higher modes were found to be characteristic of sandwich behavior. That is, they are dominated by the deformation of either the core or the faces.
2. The electric potential in the piezoelectric faces was found to be slightly quadratic only for the last four modes dominated by the deformations of the faces. Quadratic electric potential is necessary for satisfying the electric charge equilibrium equation, as demonstrated in Rahmoune et al. (1998) using a mathematical asymptotic technique.
3. Only the global modes can be well represented by a mixed ESL/layerwise modeling approach; i.e. with a unique displacement field and layerwise electric potential. The latter was necessary for all modes of the hybrid plate. Hence, these results validate the electromechanical full layerwise assumptions retained in the present closed-form solution.

4. The sandwich modes, dominated by either the core or the faces deformations, can be explicitly characterized by the faces mean and relative in-plane displacements and bending rotations. Augmented by the deflection, they can be retained as independent variables for developing a simple and accurate adaptive sandwich plate FE.
5. Both frequencies and through-thickness distributions of the mechanical displacements and electric potential are very accurate with regards to the corresponding exact 3D state space solution, implemented for comparison purpose. In particular, the first five 2D thickness modes correspond to the 3D ones within 3% maximum error.

The present 2D closed-form solution has been already used for physical understanding of the electromechanical behavior of piezoelectric adaptive sandwich plates, for which this analysis has shown the necessity of a full layerwise modeling. It is clear then, as was demonstrated in the validation and analysis sections, that it can be useful as a reference for development or validation of other 2D approximate analytical or numerical approaches, in particular for 2D piezoelectric adaptive FEs. For the latter, this kind of analytical solution is more suitable to be taken as reference since it eliminates the intrinsic error due to the 2D approximation. The present approach is currently being extended to consider the shear actuation/sensing mechanism obtained with in-plane polarized piezoelectric materials (Benjeddou, 2000b,c).

Appendix A. Zero-normal stress reduced piezoelectric constitutive equations

The 3D constitutive equations (Eq. (5)) applied to an orthotropic piezoelectric material can be written in its material axes (1,2,3), using the usual condensed (engineering) notations for the material constants as,

$$\begin{Bmatrix}\sigma_{11}\\ \sigma_{22}\\ \sigma_{33}\\ \sigma_{23}\\ \sigma_{13}\\ \sigma_{12}\end{Bmatrix}=\begin{bmatrix}C_{11} & C_{12} & C_{13} & 0 & 0 & 0\\ C_{12} & C_{22} & C_{23} & 0 & 0 & 0\\ C_{13} & C_{23} & C_{33} & 0 & 0 & 0\\ 0 & 0 & 0 & C_{44} & 0 & 0\\ 0 & 0 & 0 & 0 & C_{55} & 0\\ 0 & 0 & 0 & 0 & 0 & C_{66}\end{bmatrix}\begin{Bmatrix}\varepsilon_{11}\\ \varepsilon_{22}\\ \varepsilon_{33}\\ \gamma_{23}\\ \gamma_{13}\\ \gamma_{12}\end{Bmatrix}-\begin{bmatrix}0 & 0 & e_{13}\\ 0 & 0 & e_{23}\\ 0 & 0 & e_{33}\\ 0 & e_{24} & 0\\ e_{15} & 0 & 0\\ 0 & 0 & 0\end{bmatrix}\begin{Bmatrix}E_1\\ E_2\\ E_3\end{Bmatrix} \tag{A.1a}$$

$$\begin{Bmatrix}E_1\\ E_2\\ E_3\end{Bmatrix}=\begin{bmatrix}0 & 0 & 0 & 0 & e_{15} & 0\\ 0 & 0 & 0 & e_{24} & 0 & 0\\ e_{13} & e_{23} & e_{33} & 0 & 0 & 0\end{bmatrix}\begin{Bmatrix}\varepsilon_{11}\\ \varepsilon_{22}\\ \varepsilon_{33}\\ \gamma_{23}\\ \gamma_{13}\\ \gamma_{12}\end{Bmatrix}+\begin{bmatrix}\epsilon_{11} & 0 & 0\\ 0 & \epsilon_{22} & 0\\ 0 & 0 & \epsilon_{33}\end{bmatrix}\begin{Bmatrix}E_1\\ E_2\\ E_3\end{Bmatrix} \tag{A.1b}$$

Due to the zero-normal stress assumption of the FSDT and decomposing the stresses and electric displacements into in-plane and transverse components, the converse piezoelectric constitutive equation, Eq. (A.1a), reduces to,

$$\begin{Bmatrix}\sigma_{11}\\ \sigma_{22}\\ \sigma_{12}\end{Bmatrix}=\begin{bmatrix}C^*_{11} & C^*_{12} & 0\\ C^*_{12} & C^*_{22} & 0\\ 0 & 0 & C_{66}\end{bmatrix}\begin{Bmatrix}\varepsilon_{11}\\ \varepsilon_{22}\\ \gamma_{12}\end{Bmatrix}-\begin{Bmatrix}e^*_{31}\\ e^*_{32}\\ 0\end{Bmatrix}E_3 \quad \text{or} \quad \{\boldsymbol{\sigma}\}=[\mathbf{C}^*]\{\boldsymbol{\varepsilon}\}-\{\mathbf{e}^*_t\}E_3 \tag{A.2a}$$

$$\begin{Bmatrix}\sigma_{23}\\ \sigma_{13}\end{Bmatrix}=\begin{bmatrix}C_{44} & 0\\ 0 & C_{55}\end{bmatrix}\begin{Bmatrix}\gamma_{23}\\ \gamma_{13}\end{Bmatrix}-\begin{bmatrix}0 & e_{24}\\ e_{15} & 0\end{bmatrix}\begin{Bmatrix}E_1\\ E_2\end{Bmatrix} \quad \text{or} \quad \{\boldsymbol{\tau}\}=[\mathbf{C}_s]\{\boldsymbol{\gamma}\}-[\mathbf{e}_s]^T\{\mathbf{E}_p\} \tag{A.2b}$$

with

$$C^*_{\alpha\beta} = C_{\alpha\beta} - C_{\alpha 3}C_{\beta 3}/C_{33}, \quad e^*_{3\alpha} = e_{3\alpha} - e_{33}C_{\alpha 3}/C_{33}$$

Similarly, the direct piezoelectric constitutive equation, Eq. (A.1b), reduces to,

$$\begin{Bmatrix} D_1 \\ D_2 \end{Bmatrix} = \begin{bmatrix} 0 & e_{15} \\ e_{24} & 0 \end{bmatrix} \begin{Bmatrix} \gamma_{23} \\ \gamma_{13} \end{Bmatrix} + \begin{bmatrix} \epsilon_{11} & 0 \\ 0 & \epsilon_{22} \end{bmatrix} \begin{Bmatrix} E_1 \\ E_2 \end{Bmatrix} \quad \text{or} \quad \{\mathbf{D}_p\} = [\mathbf{e}_s]\{\boldsymbol{\gamma}\} + [\epsilon_p]\{\mathbf{E}_p\} \tag{A.3a}$$

$$D_3 = (e^*_{31}\varepsilon_{11} + e^*_{32}\varepsilon_{22}) + \epsilon^*_{33}E_3 \quad \text{or} \quad D_3 = \langle \mathbf{e}^*_t \rangle \{\boldsymbol{\varepsilon}\} + \epsilon^*_{33}E_3 \tag{A.3b}$$

with

$$\epsilon^*_{33} = \epsilon_{33} - e_{33}e_{33}/C_{33}$$

References

Batra, R.C., Liang, X.Q., 1997. The vibration of a rectangular laminated elastic plate with embedded piezoelectric sensors and actuators. Computers and Structures 63 (2), 203–216.

Benjeddou, A., 2000a. Advances in piezoelectric finite element modeling of adaptive structural elements: a survey. Computers and Structures 76 (1–3), 347–363.

Benjeddou, A., 2000b. Piezoelectric transverse shear actuation of shells of revolution: theoretical formulation and analysis. In: CD-ROM Proceedings of the European Congress on Computational Methods in Applied Sciences and Engineering. ECCOMAS, Barcelona (Invited Lecture).

Benjeddou, A., 2000c. Transverse shear piezoelectric actuation of shells. In: CD-ROM Proceedings of the Fourth International Colloquium on Computation of Shell and Spatial Structures. ISASR-NTUA, Athens.

Correia, V.M.F., Gomes, M.A.A., Suleman, A., Soares, C.M.M., Soares, C.M.M., 2000. Modelling and design of adaptive composite structures. Computer Methods in Applied Mechanics and Engineering 185, 325–346.

Ding, H.J., Chen, W.Q., Xu, R.Q., 2000. New state space formulations for transversely isotropic piezoelectricity with applications. Mechanics Research Communications 27 (3), 319–326.

Heyliger, P., Saravanos, D.A., 1995. Exact free-vibration analysis of laminated plates with embedded piezoelectric layers. Journal of the Acoustical Society of America 98 (3), 1547–1557.

Krommer, V.M., Irschik, H., 2000. A Reissner–Mindlin type plate theory including the direct piezoelectric and the pyroelectric effect. Acta Mechanica 141, 51–69.

Mitchell, J.A., Reddy, J.N., 1995. A refined hybrid plate theory for composite laminates with piezoelectric laminae. International Journal of Solids and Structures 32 (16), 2345–2367.

Rahmoune, M., Benjeddou, A., Ohayon, R., Osmont, D., 1998. New thin piezoelectric plate models. Journal of Intelligent Material Systems and Structures 9 (12), 1017–1029.

Saravanos, D.A., Heyliger, P.R., 1999. Mechanics and computational models for laminated piezoelectric beams, plates and shells. Applied Mechanics Reviews 52 (10), 305–320.

Saravanos, D.A., Heyliger, P.R., Hopkins, D.A., 1997. Layerwise mechanics and finite element for the dynamic analysis of piezoelectric composite plates. International Journal of Solids and Structures 34 (3), 359–378.

Shen, S., Kuang, Z.B., 1999. An active control model of laminated piezothermoelastic plate. International Journal of Solids and Structures 36, 1925–1947.

Srinivas, S., Rao, C.V.J., Rao, A.K., 1970. An exact analysis for vibration of simply-supported homogeneous and laminated thick rectangular plates. Journal of Sound and Vibration 12 (2), 187–199.

Tiersten, H.F., 1969. Linear Piezoelectric Plate Vibrations. Plenum Press, New York.

Xu, K., Noor, A.K., Tang, Y.Y., 1997. Three-dimensional solutions for free-vibrations of initially stressed thermoelectromechanical multilayered plates. Computer Methods in Applied Mechanics and Engineering 141, 125–139.